

The commissioning of and first results from the UIST imager spectrometer

S. Ramsay Howat^{*a}, Stephen Todd^a, Sandy Leggett^b, Chris Davis^b, Mel Strachan^a, Alastair Borrowman^a, Maureen Ellis^a, Jim Elliot^a, David Gostick^a, Russell Kackley^b, Matthew Rippa^b

^aUK Astronomy Technology Centre, Royal Observatory, Blackford Hill, Edinburgh EH9 3HJ, U.K.

^bJoint Astronomy Centre, 660, N. A'ohuku Place, University Park, Hilo, Hawaii 96720, U.S.A.

ABSTRACT

UIST is a facility class near-infrared instrument recently commissioned at the UK Infrared Telescope (UKIRT). UIST provides a comprehensive imaging and spectroscopic facility with spatial resolution limited only by the delivered tip-tilt corrected seeing. In addition to long slit spectroscopic modes, UIST includes the first deployable cryogenic integral field unit in a common user instrument. We will present results obtained during the commissioning period in late 2002. These include measurements of the image quality and the sensitivities of the different observing modes of the instrument. We also discuss the use of an instrument-specific telescope pointing-model developed for UIST to allow the instrument to meet the stringent flexure requirements arising from the choice of 0.06arcsec/pixel and 0.12arcsec/pixel plate scales. We pay particular attention to the performance of the image slicing integral field unit (IFU). We will present astronomical results from the first year of UIST operations, during which time UIST carried out diverse programmes, from mineralogical studies of Mars to measuring the mass of the black hole at the centre of the most distant quasar.

Keywords: near-infrared instrumentation, integral field spectroscopy, telescope pointing, flexure control, cryogenic instruments

1. INTRODUCTION

The new UKIRT Imager-Spectrometer (UIST) was designed and built at the UK Astronomy Technology Centre and delivered to the Joint Astronomy Centre in August 2002. UIST was designed¹ to exploit the image quality delivered by the UKIRT Upgrades programme². The image quality enhancements delivered by this have resulted in a median seeing at UKIRT of 0.6arcsec with the 20th-percentile value being 0.4arcsec³. UIST offers a number of different scientific modes as follows:

- imaging with plate scales of 0.12arcsec and 0.06arcsec per pixel and a pupil imaging mode;
- imaging through broad and narrow band filters;
- JHKLM spectroscopy, complete coverage of each atmospheric window with R~500-1500 for a 0.24arcsec slit;
- JHK spectroscopy with R~3000-4000 for a 0.24arcsec slit;
- integral field spectroscopy with a deployable image slicer over a 3.3arcsec x 6.0arcsec field;
- imaging and spectro-polarimetry with a 20arcsec field.
-

UIST was delivered with all of these modes operational.

The layout of the instrument is shown in Figure 1. The mechanical design is highly modular. Each module is made from aluminium, mounted on an aluminium support structure which also acts as an optical bench for instrument alignment. The design has been detailed in an early paper¹. All of the powered optics in the main optical train are refractive and use glasses whose performance in cryogenic instruments is proven, BaF₂, CaF₂, LiF and ZnSe. The largest optical component is the CaF₂ window (140mm diameter). An image rotator ahead of the slit focal plane allows the slit position angle of the sky to be selected, as UKIRT has no instrument rotator. The collimated beam at the filter wheel is 15mm, allowing the use of 25mm filters. The imaging filters were procured through the Gemini filter consortium⁴.

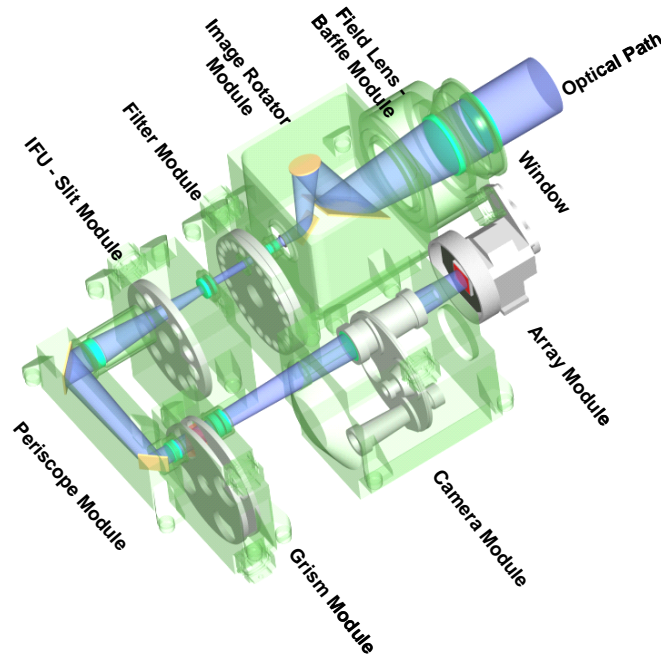


Figure 1: A schematic layout of UIST.

The slit wheel contains slits of a variety of widths from 0.24arcsec to 0.84arcsec as well as masks for the imaging field of view and for the polarimetry. After the 30mm collimated beam is folded by a periscope module consisting of two gold-coated, diamond-machined Al mirrors, it passes through the grism wheel. Two wheels contain a total of 10 grisms and a Wollaston prism. The grisms are of two types. The high resolution grisms and the L and M band grisms are made from prisms of KRS5 with the grating directly ruled onto the prism (from Carl Zeiss, Jena). The low resolution grism covering the HK wavelength bands is from infrared fused silica (Infrasil) with the grating replicated into an epoxy layer on the surface of a prism (from Hyperfine). The three cameras consist of two doublets. One doublet is common to all and is fixed onto the front of the grisms module. The second doublet is exchanged to change the plate scale. The 0.12arcsec plate scale is provided by one doublet. The 0.06arcsec plate scale is provided by two doublets, one for the J, L and M wavelength bands, the second for H and K. This compromise allowed use to reuse a proven focus mechanism design⁵, developed for the GMOS instrument, which is restricted to 5mm total travel along the optical axis. The UIST detector is a 1024x1024 Aladdin II InSb array from Raytheon. The instrument is pre-cooled using liquid nitrogen and then the cryogenic temperatures maintained by a closed cycle cooler (CCC). The main optical bench reaches an equilibrium temperature of 60K. The array is attached to the second stage of the CCC reaches <20K. It is heated to its operating temperature (30K) using a heater mounted behind the array under closed loop control; this provides stability of the array temperature and consequently of the dark current.

2. ON SKY PERFORMANCE

UIST was delivered to the Joint Astronomy Centre in August 2002, subsequently achieving first light on the telescope on 25th September 2002. During the first half night, data were obtained in the three major instrument modes: imaging, spectroscopy and IFU spectroscopy. The 'end-to-end' system from observing preparation to data reduction by the automatic pipeline was complete and tested for each of these without hitch. UIST data are reduced using the UKIRT pipeline reduction software, ORAC-DR⁶. The UIST pipeline uses code modified from that for UFTI and CGS4 for imaging and spectroscopy and can also reduce integral field unit data, producing flat-fielded, flux calibrated datacubes⁷.

The commissioning period was 20 nights duration distributed through the months to early December, when the first observing time was available to the astronomy community on a ‘shared risks’ basis. In anticipation of promptly realising the engineering requirements of the commissioning time, an announcement of opportunity for observations to be executed in service mode during the commissioning had been made. The reliability of the instrument was such that observations were obtained for total of 12 service programmes.

Filter	Exposure time in seconds			
	10	60	600	3600
1.25 um/J	17.7	18.7	20.0	20.9
1.65 um/H	17.0	18.0	19.3	20.2
2.2 um/K	16.6	17.6	18.9	19.8
3.8 um/L'	10.9	12.0	13.3	14.2
4.7 um/M'	8.8	9.8	11.1	12.0

Table 1: Imaging sensitivities.

The on-sky performance of the instrument confirms that the image quality achieved is limited by the seeing and not by the instrument optics. Point source sensitivities for imaging and spectroscopy are shown in Table 1 and Table 2. The overall throughput of the instrument is 50% of the predicted throughput from the UIST performance model (e.g. 20% at K band, including filters and detector QE), resulting lower sensitivity than anticipated. Using the pupil imaging mode, we are able to confirm that the cold stop matches the telescope pupil and that the pupil is not vignetted. The cause of the throughput reduction is not definitively known since no separate test of detector and optics has been possible whilst the instrument remains in constant use at the telescope.

Grism*	Wavelength	Resolution per 2 pixels	Point Source 3sig2min (mag)	Point Source 3sig5min (mag)	Point Source 3sig10min (mag)	Point Source 3sig30min (mag)
Low resolution mode						
IJ	1.25um	950	15.4	15.9	16.3	16.9
	1.05um		14.6	15.1	15.5	16.1
HK	2.20um	800-1000	15.6	16.1	16.5	17.1
	1.60um		15.6	16.1	16.5	17.1
KL	2.4um	1400	12.6	13.1	13.5	14.1
M	4.82um	2000	9.3	9.8	10.2	10.8
High resolution mode						
short J	1.08um	3000	14.3	14.8	15.2	15.8
long J	1.23um	4100	14.5	15.0	15.4	16.0
short H	1.52um	3800	14.6	15.1	15.5	16.1
long H	1.70um	4000	14.5	15.0	15.4	16.0
short K	2.13um	3600	14.0	14.5	14.9	15.5
long K	2.30um	3800	13.0	13.5	13.9	14.5
short L	3.27um	1300	9.7	10.2	10.6	11.2
long L	3.84um	2300	9.8	10.3	10.7	11.3

Table 2: Spectroscopic sensitivities (theoretical for the IJ grism).

The biggest imaging gains with UIST come in the thermal infrared, where observations are traditionally dominated by the overheads in reading out the array. The small spatial scale of the pixels allows reasonable integration times before saturating on the background. The result is larger fields of view observed more efficiently than was possible with the previous UKIRT camera (Table 3).

Camera "/pixel	Filter	Overheads		Field, arcseconds	
		1024x1024	512x512	1024x1024	512x512
0.12	L'	110%	-	123	-
0.12	L'	-	54%	-	61
0.06	L'	38%	14%	62	31
0.12	M'	-	100%	N/A	61
0.06	M'	56%	18%	62	31

Table 3: Thermal imaging parameters.

2.1. Array performance

The performance achieved with the UIST array is summarised as follows. A non-destructive read algorithm is used to reduce the read-noise. A sample of the signal is taken every second during an exposure; each sample has six reads, averaged. For a double correlated sample, the read-noise is 38electrons; the graph for the reduction in noise with the number of reads is shown in Figure 2. The read-noise reaches a plateau after 50 samples, at 15electrons. The UIST array is operated with two bias voltages and two clock rates for thermal imaging and non-thermal imaging plus spectroscopy. For the thermal infrared (LM bands) a 900mV bias is set providing a deep well (2.4×10^5 electrons); the clock speed is set to give a minimum read time of 0.21s for the full array. For all other modes, a 600mV bias gives a well depth of 1.5×10^5 electrons and the clock speed sets a minimum read time of 1.0s. Increasing the clock speed increases the observed array 'cross-talk' - the signal on one column is echoed eight columns later. The thermal imaging mode is a compromise between read-out speed and cross-talk (<2% for the thermal clock speed). Persistent images are also seen with these arrays. During a 0.2s idle period before each exposure the array is reset to reduce the residual image.

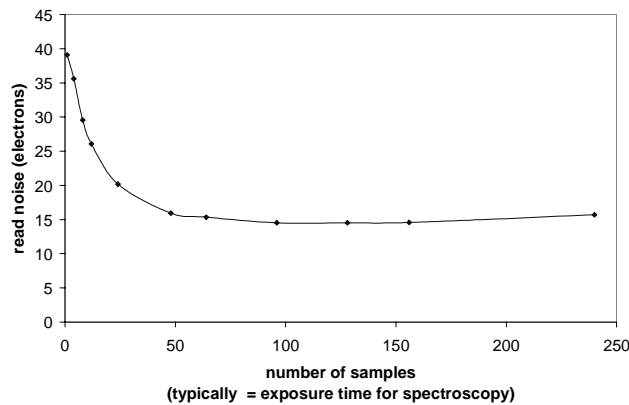


Figure 2: Read-noise reduction for multiple non-destructive reads.

2.2. Performance of the telescope pointing model

The moderately high spatial resolution required to meet the UIST science requirements provided some significant challenges for controlling the pointing of the instrument plus telescope system. The autoguider on UKIRT senses the optical beam directed through a dichroic tertiary mirror located in front of the telescope focal plane. The infrared beam is directed into the instrument. Any differential offset between the guider and the instrument focal plane will allow the source to move on the narrow UIST slits or will degrade the image quality during long integrations. A differential offset would be introduced either by flexure of the telescope dichroic and instrument support structure or flexure of the instrument mounting. During the UIST design phases, we verified using the UFTI camera that the telescope flexure was significant compared with the UIST requirements, but, importantly, that it was repeatable and a simple function. In preference to re-engineering the telescope and building stiff and heavy mounting struts for UIST, our philosophy for

dealing with these guiding errors was to adopt an instrument specific pointing model for UIST. The concept is as follows. The mechanical design of the optical bench and internal components ensures that the motion of the slit focal plane to the detector is kept to less than 0.2pixel motion over a 15degree change in telescope attitude. This was confirmed during lab testing of the instrument. The motion of UIST on its mounting struts was designed and confirmed to be repeatable and represented by a simple function⁸. Motions of the source on the slit are corrected using the pointing model.

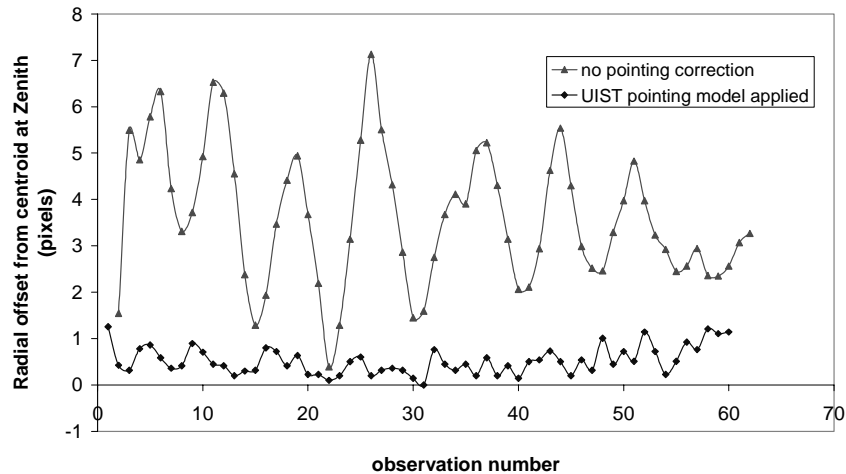


Figure 3: Pointing offsets before and after application of the correction.

This was accomplished by making use of the capability built into the UKIRT Telescope Control System (TCS) to specify one pointing model to control the telescope beam position on UIST and a second pointing model to control the beam position on the guide camera. This capability was inherent in the TCS because it makes use of the virtual telescope concept⁹. The TCS implements both a main virtual telescope, which determines the beam position on UIST, and a guide virtual telescope, which determines the beam position on the guide camera. The two virtual telescopes can be controlled independently. Each virtual telescope can have its own target coordinates, differential tracking rates, pointing model, etc. Since UKIRT typically supports a suite of three or four instruments and only UIST requires a specific pointing model, the TCS was modified slightly so that it incorporated additional pointing terms on an instrument-specific basis.

During commissioning, the data were generated to specify the characteristics of each pointing model, following the standard UKIRT pointing checks. For 60 pointings over the sky, a bright star was centred on the guide probe and the required telescope offsets noted. Using the TPOINT¹⁰ software, a set of twelve pointing terms was generated by analysing the difference between the observed and known coordinates. This is the guide probe pointing model. Simultaneously, the centroid of the star is measured by UIST and the offset from the fiducial pixel on the array obtained. These centroids provide the UIST pointing model, once analysed using TPOINT to generate a further seven pointing terms. The main telescope pointing model was computed by starting with the guide telescope pointing model and applying the seven UIST terms as pointing offsets.

The positional accuracy of the telescope beam on the UIST array was analysed before and after the seven offset terms were applied to the main telescope pointing model. Before the terms were applied, the standard deviation of the positional error was approximately 0.6 arcsec. After the terms were applied, the standard deviation of the positional error was approximately 0.07 arcsec (Figure 3), nearly an order-of-magnitude improvement and within the requirements for positioning on the slit. Therefore, the addition of the main virtual telescope pointing model significantly improved the positional accuracy of the telescope beam on the UIST array.

2.3. On sky performance of the UIST integral field unit

UIST is one of a handful of instruments to provide an integral field mode as a common-user facility (e.g. GMOS¹¹ and FLAMES¹² at optical wavelengths), and the first facility instrument to be offered to the astronomical community in the near-infrared (1-5 μ m). The earliest example of an infrared integral field spectrograph was 3D¹³, a fixed IFU spectrograph using an image slicer. Instruments using fibre IFUs in the infrared have included CIRPASS¹⁴ and SMIRFS¹⁵. Two newly commissioned instruments have image slicing integral field units with excellent performance in the infrared, the Gemini near-infrared spectrograph and SPIFFI¹⁶. A second Gemini spectrometer, NIFS¹⁷, will also use an image slicer. Image slicers are generally preferred due to the largely untested performance of fibres at cryogenic temperatures and the improved packing of spectra on the array.

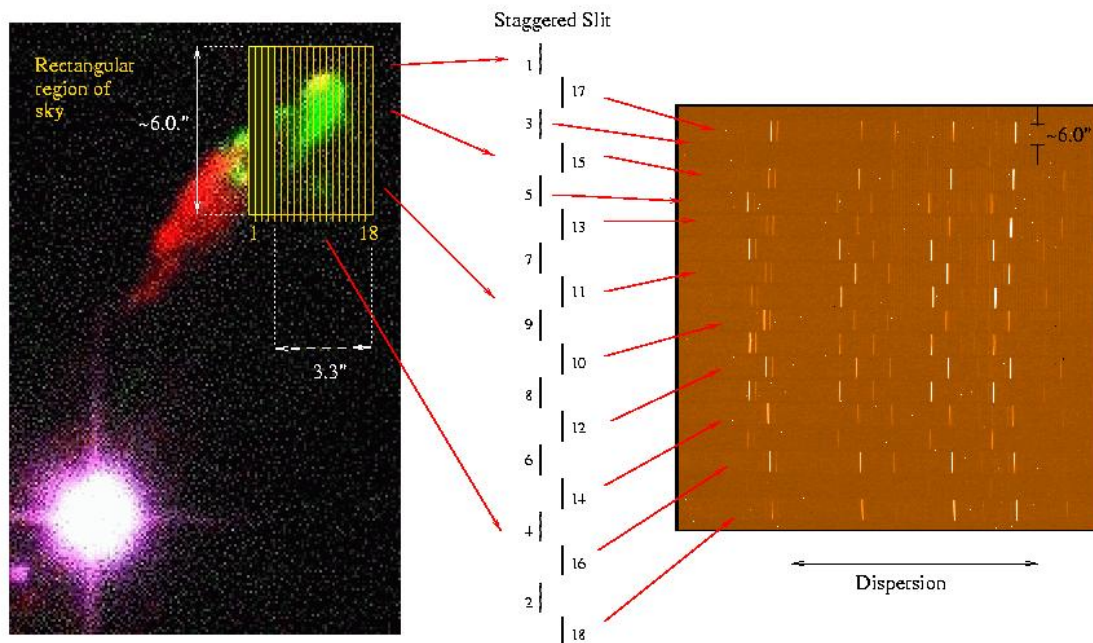


Figure 4: A schematic of the operation of the integral field unit.

The UIST integral field unit uses an image slicer and re-imaging mirrors to reformat a square array of 18 slices of the sky, each 0.24arcsec x 6.0arcsec, onto a pseudo-long slit (Figure 4). The design and lab performance of the integral field unit have been presented previously⁷. The IFU is located on the slit wheel, selected in the same way as any other focal plane mask and can be oriented on the sky using the image rotator. At the completion of the lab testing at UK ATC, the spectral image quality of the IFU was understood and the transmission relative to the long slit had been measured using the UIST calibration unit (Figure 5). Fourteen of the eighteen slices are well aligned optically, the remaining four are misaligned and the light from them is vignetted in the IFU. The resulting field of view is 3.4 x 6arcsec. The two main commissioning tasks for the IFU were to finalise the measurements of the stellar PSF measured with the IFU and to explore the relative efficiency of using the IFU and the long slit.

Each slice of the integral field unit offsets the image of a star on the detector, resulting in a shift along the long axis of the slitlet when the image is reconstructed. The design offsets were known in advance. The real offsets, which include the cumulative tolerances on the mirrors, were obtained by translating a stellar image across the integral field unit (from slice to slice) using the telescope offsets. A pair of images of the star was obtained, offsetting the telescope 3arcsec along the slice between them. When those images are subtracted, an image like that in Figure 6(a) is obtained. The seeing disk, split across two slices, appears quite disjoint. In Figure 6(b), a series of such images is coadded. The break

after 5 slices is indicative of the manufacture of the slicer mirror. Two sets of nine slices were polished simultaneously, separated in their mount by a central spacer that was removed before assembly of the slicer mirror⁷.

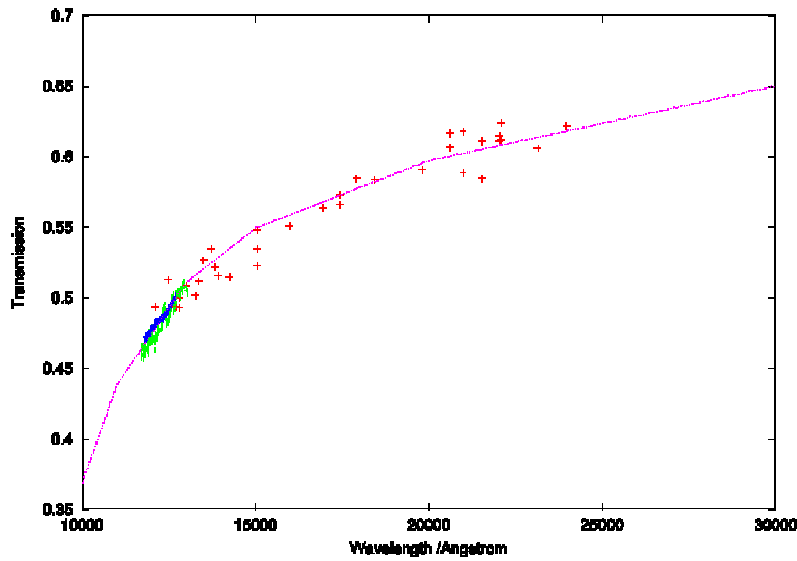


Figure 5: Transmission of the IFU relative to the two pixel wide slit, measured in the lab.

The offsets required to correct the PSF were calculated, and that correction incorporated into the data reduction pipeline. Two further corrections are required: to correct changes in the plate scale for each slice and in the magnification of the image when changing grism. Both of these introduce shifts of the order of 1 pixel at the detector. With these offsets applied the reconstructed PSF is of good quality. An analysis of 26 images showed ellipticity of 1.15 and a FWHM of the image of 0.42arcsec, consistent with the measured seeing on the night. Figure 7 shows a cross-cut through the PSF of a reconstructed star with a FWHM of 0.42arcsec. The fitted function is of the form $D \propto \exp[-0.5(r/\sigma)^{1.7}]$.

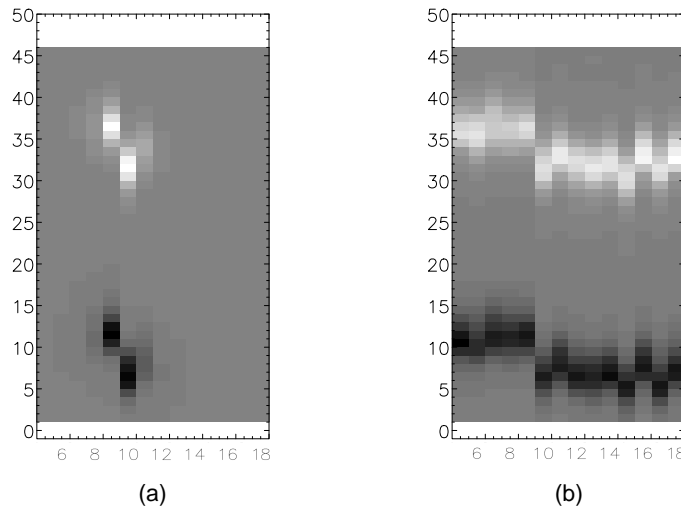


Figure 6: Coadded images showing the position of a star translated across the IFU field of view.

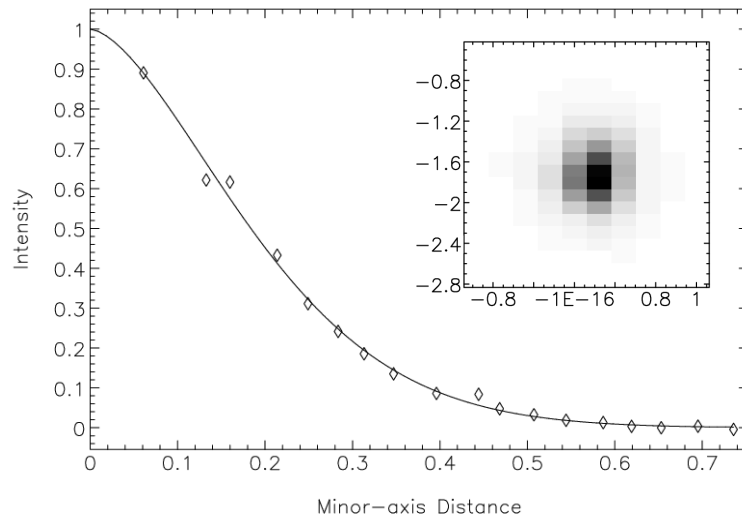


Figure 7: The PSF of a reconstructed stellar image.

One use of IFUs that was explored was the possibility of compensating for slit losses. There is an argued advantage to using an integral field unit even for point-sources in conditions of poorer seeing. Rather than use a wider slit, the IFU gathers all the light from the point source and maintains the spectral resolution of a narrow slit. We have considered the limits in which this is a useful advantage. Figure 8 shows the ratio of the time taken to observe a given point source with the IFU compared with the long slit. It assumes that separate IFU sky frames are required for the IFU but that the point source is offset along the slit. For the 70% of observations when the seeing is better than 0.7arcsec^3 , the long slit remains the best choice for point sources. For observations at wavelengths in the H band and longer, the IFU will offer gains for the 30% of time that the seeing is worse than 0.7arcsec . If the option of offsetting along the IFU can be used, then the IFU is fastest for all but the best 20% of observations. Of course, in conditions of poor seeing, offsetting along the 3.4arcsec IFU field may not be possible.

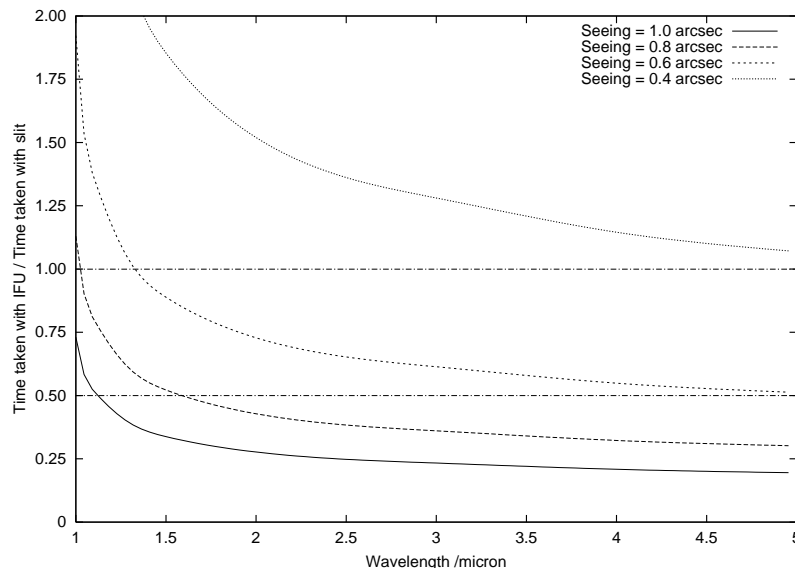


Figure 8: A comparison of the slit performance versus the integral field unit for various seeing conditions.

3. EARLY SCIENCE RESULTS FROM UIST

3.1. Imaging: Mars at closest approach

During 2003, Mars was the target of a concerted campaign of observations, thanks to the closest approach of this planet to the Earth. The infrared wavelength region contains a number of important diagnostics of the atmosphere and mineral content, e.g. CO₂ and CO₂ ice, H₂O and H₂O ice as well as more exotic minerals (hydrated clays, carbonates and sulphates). Bailey et al.¹⁸ used both imaging and spectroscopy with UIST to explore the planet with spatial resolution of less than 100km at the surface. The image shown in Figure 9 is obtained after co-adding the best images obtained during very rapid (0.09second) exposures with the UIST 0.06arcsec camera then using the technique of “unsharp masking” to maximise the spatial resolution. Whilst ground-based images cannot match the spatial resolution obtained by orbiting missions, they do reveal the structures which are familiar from those missions and offer the real possibility of monitoring seasonal changes in the Martian atmosphere. Scanning the long slit across the disk of the planet, 3D datacubes of the surface have been obtained from 1-3.6 μ m. At the South Polar Cap, the HK spectrum is dominated by absorption from CO₂ ice, seen also in the image. In the North, water ice clouds in the North Polar Hood are the dominant feature, though some CO₂ ice features are also seen. The analysis of the spectral data is ongoing, searching for the hydrated molecules that are expected to reveal more about the presence of liquid water on Mars.

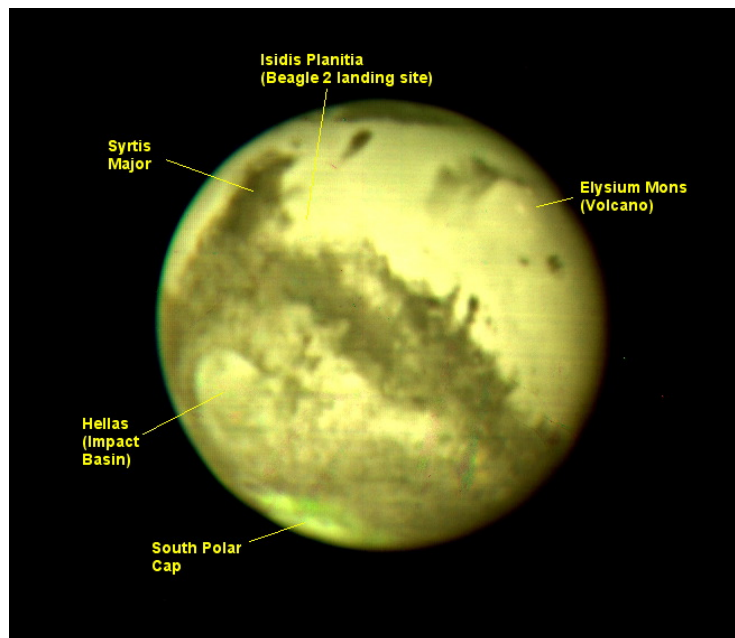


Figure 9: Mars imaged by UIST in August 2003 (Bailey et al.¹⁸).

3.2. Long-slit spectroscopy: the highest redshift quasar

Use of the HK grism for either long slit or IFU spectroscopy is the most requested UIST observing mode. The broad wavelength coverage and good sensitivity has been exploited for galactic programmes, for simultaneous observation of a large number of spectral lines, and extragalactic programmes where the wavelength coverage samples a wide range of redshifts. The HK spectrum of the quasar SDSS J1148+525 was observed on 2003 January 10¹⁹. At the time it was the most distant object observed, at a redshift of $z=6.43$ ²⁰. At this distance, the MgII $\lambda 2799$ emission line is redshifted into the K band. This line provides two key parameters – an accurate measurement of the systemic redshift of the quasar and the mass of the quasar’s central black hole. The redshift determined from the UIST observations is $z=6.41\pm 0.01$. The

central black hole in SDSS J1148+5251 was found to have a mass of $3 \times 10^9 M_{\text{solar}}$. This, coupled with the high luminosity of the object, gives the result that the black hole is accreting matter at the theoretical maximum rate, the Eddington limit¹⁹. Both the redshift and the mass of the central black hole have since been confirmed using the Keck Telescope²¹.

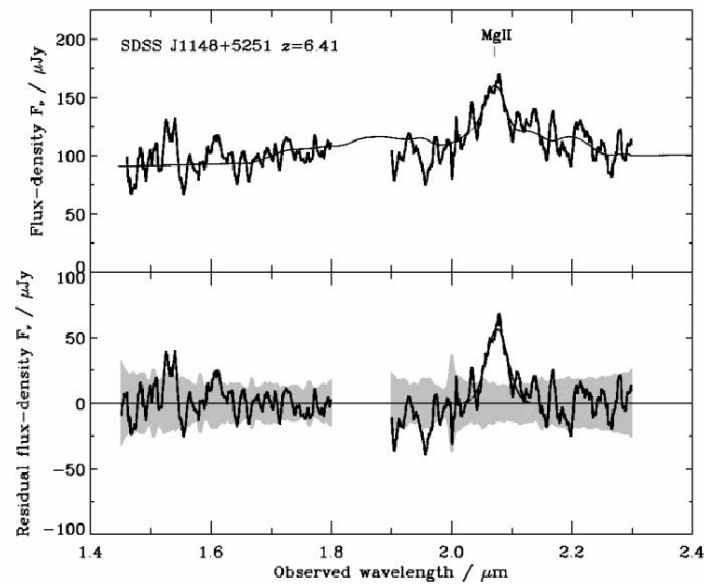


Figure 10: The HK spectrum of SDSS J1148+5251 (Willott, McClure and Jarvis 2003¹⁹).

3.3. IFU spectroscopy: Merging galaxies at $z=2.4$

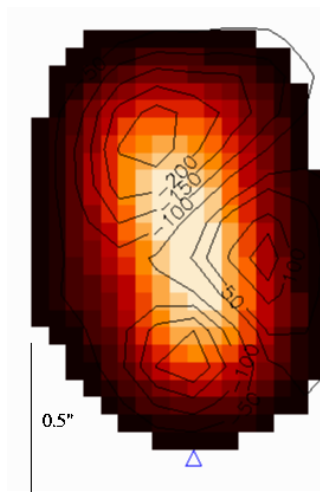


Figure 11: An $H\alpha$ map of Elais N2 850.4. (Swinbank et al, 2004²²)

Swinbank et al.²² have combined UIST and GMOS IFU¹⁰ observations to explore the formation of the Ultra Luminous Infrared Galaxy Elais N2 850.4 ($z=2.38$). Long-slit observations of this galaxy had hinted that it was a two component

merging system²³, but the 2D data were insufficient to explore fully the system dynamics. The velocity map obtained from the H α line is shown in Figure 11. The two merging systems are confirmed, their relative velocity is 400km s^{-1} . A second emission line OIII (rest wavelength 5007Å) falls within the HK grism passband. This line is offset by 1.5arcsec from the H α and also blueshifted by 700km s^{-1} and is thought to arise from AGN activity driven by the merger.

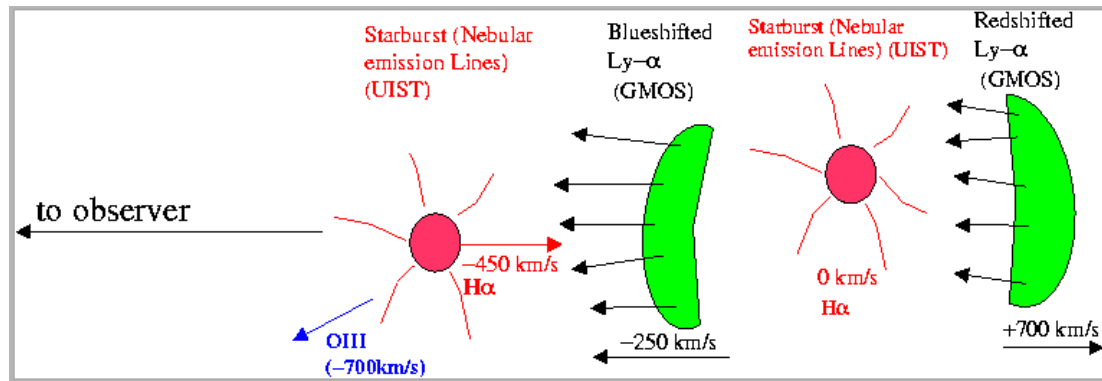


Figure 12: A cartoon of the physical processes in Elais N2 850.4.

When the UIST data are combined with GMOS IFU data, it is seen that the UV continuum is spatially coincident with the H α emission, but that the Ly α emission shows two components, offset from the two merging components. An early interpretation of these complex observations suggests the presence of an expanding shell of neutral gas, ejected from one of two merging galaxies (Figure 12).

ACKNOWLEDGEMENTS

The author list for this paper consists of the UIST commissioning team. The authors gratefully acknowledge the contribution of many people from the UK ATC and the JAC whose talents and efforts lead to the successful completion of the UIST project. Many thanks are also due to the UIST observers who have permitted their data to be reproduced here. UIST and UKIRT are funded by the Particle Physics and Astronomy Research Council.

REFERENCES

1. Ramsay Howat, S.K., Atad, E., Bennett, R., J., Bridger, A., Content, R., Ellis, M., Hastings, P., Strachan, M., Wall, R., Wells, M. 1998 SPIE Vol 3354, p456.
2. T. G. Hawarden, et al., "Upgraded UKIRT," Advanced Technology Optical/IR Telescopes VI, Proc. SPIE Vol. 3352, p. 52-61; Larry M. Stepp; Ed.; Aug 1998.
3. UKIRT seeing statistics see <http://www.jach.hawaii.edu/JACpublic/UKIRT/telescope/seeing/seeing2001.html>
4. Tokunaga, A. T. & Simons, D.A., "Mauna Kea Observatories near-infrared filter set for 1-5 microns", in "Instrument Design and Performance for Optical/Infrared Ground-based Telescopes. Edited by Iye, M. & Moorwood, A. F. M. Proc. SPIE, Vol 4841, 2003, pp. 420-424.
5. Hastings, P.R. "Focus and translation mechanism for the Gemini Multiobject Spectrograph (GMOS)" in Optical Telescopes of Today and Tomorrow, ed. by Ardeberg, A.L. Proc. SPIE, Vol 2871, 1997, p1216.
6. Bridger, A., Wright, G. S., Tan, M., Pickup, D. A., Economou, F., Currie, M. J., Adamson, A. J., Rees, N. P., Purves, M. H. "ORAC: 21st Century Observing at UKIRT" in Astronomical Data Analysis Software and Systems IX, ASP Conf. Proc., Vol. 216, ed. by N. Manset, C. Veillet, & D. Crabtree. ASP, 2000., p.467
7. Todd, S.P, Wells, M., Ramsay Howat, S.K., Hastings, P.R. "Cryogenic image slicing IFU for UKIRT: manufacture, alignment, laboratory testing, and data reduction", in Specialized Optical Developments in Astronomy. Edited by Atad-Ettdgui, E. & D'Odorico, S., Proc. SPIE, Vol 4842, 2003, pp. 151-16.
8. Gostick, D.C., Ramsay Howat, S.K. & Elliot, J.E. "Multiple Integral Field Spectroscopy Using Image Slicers", in Instrument Design and Performance for Optical/Infrared Ground-based Telescopes, ed. M. Iye & A. F. Moorwood, Proc. SPIE, Vol 4841, 2003, pp. 1315-1325.

9. J. O. Straede and P. T. Wallace, "The Anglo-Australian 3.9 meter telescope: Software controlled slewing, setting, and tracking," *Publ. Astr. Soc. Pacific* 88, pp. 792-802, 1976.
10. <http://www.tpssoft.demon.co.uk/>
11. Allington-Smith, J., Murray, G., Content, R., Dodsworth, G., Davies, R., Miller, B.W., Jorgensen, I., Hook, I., Crampton, D., Murowinski, R. "Integral Field Spectroscopy with the Gemini Multiobject Spectrograph. I. Design, Construction, and Testing" 2002, *PASP*, Vol 114, 798, pp. 892-912.
12. Pasquini, L., Alonso, J., Avila, G., Barriga, P., Biereichel, P., Buzzoni, B., Cavadore, C., Cumani, C., Dekker, H., Delabre, B., Kaufer, A., Kotzowski, H., Hill, V., Lizon, J-L, Nees, W., Santin, P., Schmutzer, R., Kesteren, A. V.; Zoccali, M. "Installation and first results of FLAMES, the VLT multifibre facility" in *Instrument Design and Performance for Optical/Infrared Ground-based Telescopes*. Edited by Iye, M., Moorwood, A. F. M. *Proc. SPIE*, Vol 4841, 2003, pp. 1682-1693.
13. Weitzel, L., Krabbe, A., Kroker, H., Thatte, N., Tacconi-Garman, L. E., Cameron, M., Genzel, R "3D: The next generation near-infrared imaging spectrometer", 1996, *A&AS*, 119, 531.
14. Parry, I.R., Mackay, C.D., Johnson, R.A., McMahon, R.G., Dean, A., Ramaprakash, A.N., King, D.L., Pritchard, J.M., Medlen, S.R., Sabbey, C.S., Ellis, R.S., Aragon-Salamanca, A. "CIRPASS: a NIR integral field and multi-object spectrograph" in *Optical and IR Telescope Instrumentation and Detectors*, Edited by Iye, M., Moorwood, A. F. M. *Proc. SPIE*, Vol 4008, 2000, pp. 1193.
15. Haynes, R., Content, R., Turner, J., Allington-Smith, J. R., Lee, D. "SMIRFS-II: multiobject and integral-field near-IR spectroscopy at UKIRT" in *Infrared Astronomical Instrumentation*, ed. A. Fowler, *SPIE*, Vol 3354, pp419-430
16. Eisenhauer, F. et al. "On-sky performance of SPIFFI: the integral field spectrometer for SINFONI at the VLT", *these proceedings*, 5492-49.
17. McGregor, P. J., J., Conroy, P. G., Pfitzner, M. L.; Bloxham, G. J., Jones, D. J., Downing, M. D., Dawson, M., Young, P.; Jarnyk, M., Van Harmelen, J. "Gemini near-infrared integral field spectrograph (NIFS)", in *Instrument Design and Performance for Optical/Infrared Ground-based Telescopes*. Edited by Iye, M., Moorwood, A. F. M. *Proc. SPIE*, Vol 4841, 2003, pp. 1581-1591.
18. Bailey, J., Chamberlain, S., Walter, M., Crisp, D., "Ground Based IR Imaging Spectroscopy of Mars" in *ESA SP-545, Proceedings of the 3rd European Exo/Astrobiology Workshop, Mars: The search for life*, 2004.
19. Willott, C., McClure, R. & Jarvis, M. "A 3×10^9 Msolar Black Hole in the Quasar SDSS J1148+5251 at $z=6.41$ ", 2003, *ApJL*, 587.
20. Fan, X. et al., "A Survey of $z > 5.8$ Quasars in the Sloan Digital Sky Survey. I. Discovery of Three New Quasars and the Spatial Density of Luminous Quasars at $z \sim 6$ ", 2001, *AJ*, 122, 6, pp. 2833-2849.
21. Barth, A.J., Martini, P., Nelson, C.H., Ho, L.C. "Iron Emission in the $z = 6.4$ Quasar SDSS J114816.64+525150.3", 2003, *ApJL*, 594, 95.
22. Swinbank, M. et al., 2004, in preparation.
23. Smail, I., Chapman, S. C., Ivison, R. J., Blain, A. W., Takata, T., Heckman, T. M., Dunlop, J. S., Sekiguchi, K. "A vigorous starburst in the SCUBA galaxy N2 850.4", 2003, *MNRAS*, 342, 1185.